



## High-resolution nanoscale NMR for arbitrary magnetic fields

Jonas Meinel <sup>1,2</sup>, MinSik Kwon<sup>1,2</sup>, Rouven Maier <sup>1,2</sup>, Durga Dasari<sup>1</sup>, Hitoshi Sumiya<sup>3</sup>, Shinobu Onoda<sup>4</sup>, Junichi Isoya<sup>5</sup>, Vadim Vorobyov <sup>1✉</sup> & Jörg Wrachtrup<sup>1,2</sup>

Nitrogen vacancy (NV) centers are a major platform for the detection of nuclear magnetic resonance (NMR) signals at the nanoscale. To overcome the intrinsic electron spin lifetime limit in spectral resolution, a heterodyne detection approach is widely used. However, application of this technique at high magnetic fields is yet an unsolved problem. Here, we introduce a heterodyne detection method utilizing a series of phase coherent electron nuclear double resonance sensing blocks, thus eliminating the numerous Rabi microwave pulses required in the detection. Our detection protocol can be extended to high magnetic fields, allowing chemical shift resolution in NMR experiments. We demonstrate this principle on a weakly coupled  $^{13}\text{C}$  nuclear spin in the bath surrounding single NV centers, and compare the results to existing heterodyne protocols. Additionally, we identify the combination of NV-spin-initialization infidelity and strong sensor-target-coupling as linewidth-limiting decoherence source, paving the way towards high-field heterodyne NMR protocols with chemical resolution.

<sup>1</sup>3rd Institute of Physics, University of Stuttgart, 70569 Stuttgart, Germany. <sup>2</sup>Max Planck Institute for Solid State Research, 70569 Stuttgart, Germany.

<sup>3</sup>Advanced Materials Laboratory, Sumitomo Electric Industries Ltd., Itami, Hyogo 664-0016, Japan. <sup>4</sup>Takasaki Advanced Radiation Research Institute, National Institutes for Quantum and Radiological Science and Technology, 1233 Watanuki, Takasaki, Gunma 370-1292, Japan. <sup>5</sup>Faculty of Pure and Applied Sciences, University of Tsukuba, Tsukuba, Ibaraki 305-8550, Japan. ✉email: [v.vorobyov@pi3.uni-stuttgart.de](mailto:v.vorobyov@pi3.uni-stuttgart.de)

Nuclear magnetic resonance (NMR) is one of the most powerful analytical tools in medicine, chemistry, material science and physics<sup>1</sup>. Various attempts have been made to increase the sensitivity of the method to decrease the required sample sizes from millimeter to the micro- or even nanoscales<sup>2</sup>. One of the promising avenues is the use of optically addressable paramagnetic centers, e.g. NV centers in diamond as sensors (illustrated in Fig. 1a). By combining high fidelity readout and long coherence times, NV centers provide an excellent platform for sensing of NMR signals. The optically detectable electron spin of the NV center allows for single electron spin detection at room temperature. Such single electron spins or a small ensemble of electron spins are used as nanoscale probes of their local environment, e.g. the magnetic field of a set of nuclei. Experiments rely on the observation of (modified) electron spin echo envelope modulation signals (ESEEM), e.g. using dynamical decoupling sequences such as Carr-Purcell-Meiboom-Gill (CPMG) and Knill dynamical decoupling<sup>3</sup>. In these techniques the precessing nuclear spins generate a time varying magnetic field at the location of the spin via the off-diagonal hyperfine coupling elements ( $B_z = B(I_x, I_y) \cos(\omega_L t)$ )<sup>4</sup>. This time varying field is detected by these pulse sequences, if e.g. the pulse spacing in a CPMG sequence is exactly commensurate with  $\omega_L$ . These techniques were extended to correlation type sequences, e.g. 5 pulse ESEEM<sup>5,6</sup>, or correlation CPMG sequences<sup>7</sup>, with the possibility to increase the available correlation time to the ancillary nuclear spin memory lifetime used in the experiment<sup>6,8</sup>. However, in all of these techniques an intrinsic quantum sensor spin relaxation time  $T_1$  is the fundamental limit of the achievable spectral resolution for NMR signals. One method to overcome the limitation imposed by the quantum sensor  $T_1$  decay is the use of sequential measurements<sup>9–12</sup> (see Fig. 1b). Each measurement is composed of electron spin initialisation, coherent interaction with the target

nuclear spin during the electron pulse sequence and optical electron spin readout. Here one uses the fact that nuclear oscillations persist longer than the NV electron  $T_1$ . Rather than probing this oscillations with a single run of an electron spin detection sequence, one can use multiple of those measurement runs and sample the nuclear oscillation in a phase coherent manner (see Fig. 1b). This technique has become state of the art in high resolution methods denoted as quantum heterodyne (qdyne) or coherent averaged synchronised readout (CASR)<sup>13</sup>, which has demonstrated a spectral resolution only limited by the external clock used to synchronize the pulse sequence. However, this technique requires the repeated application of MW- $\pi$ -pulses to the electron spin, which need to be faster than the corresponding nuclear Larmor frequency to avoid a severe loss of sensitivity<sup>4</sup>. At a field of 3 T for example, the Larmor frequency of a proton spin is 120 MHz. Application of the sequential measurement scheme would thus require the application of pulses on the NV electron spin with pulse length well below 8 ns, which is technically hard to achieve. As a result, the conventional qdyne detection schemes are intrinsically difficult to extend to high magnetic fields, where however chemical shift and J-coupling resolution<sup>14</sup> is easiest. Further on, at high-field NMR the thermal polarization becomes comparable to the statistical polarization already in smaller sample volumes, which would allow overcoming the diffusion limit of spectral resolution.

Recently, a heterodyne sensing principle was applied to high frequency signals, e.g. in the microwave band. By utilizing the interaction of an oscillating microwave field with the spin in the rotating frame, the signal is correlated to the phase of the external ref.<sup>15–17</sup>.

In this work, we utilize this effect for a proof-of-principle heterodyne detection of NMR signals at moderate fields ( $B = 0.25$  T). Rather than probing the nuclear  $I_x$  and  $I_y$

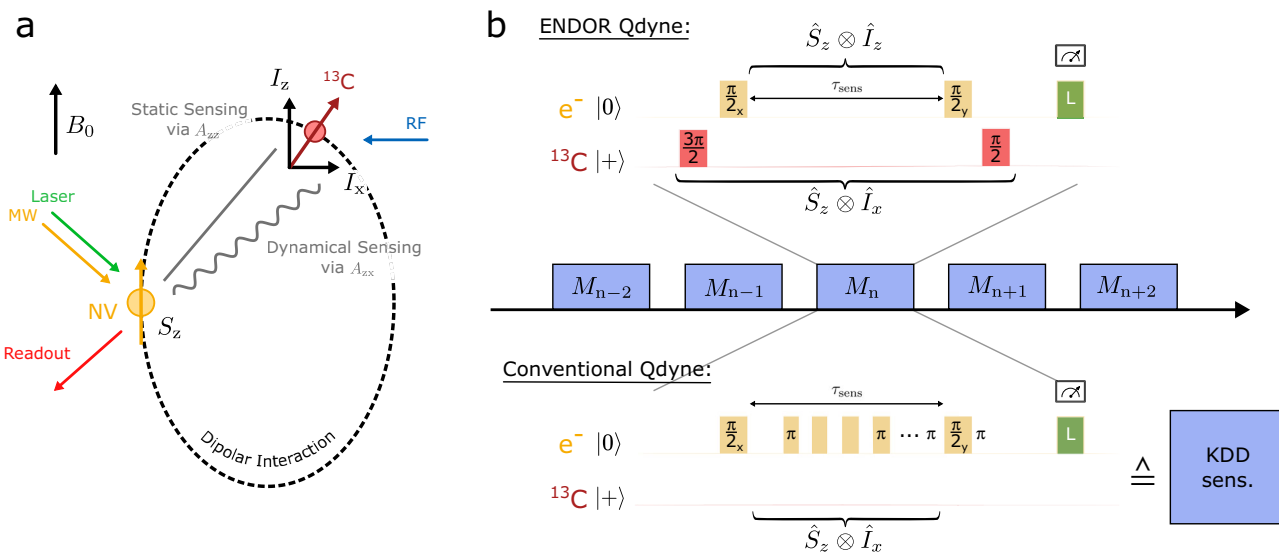


**Fig. 1** Concept of field independent heterodyne sensing by coherent sequential double resonance. **a** The Nitrogen vacancy (NV) center with its internal  $^{13}\text{C}$  is studied as a nano-scale surface Nuclear Magnetic Resonance (NMR) experiment with a diamond sensor. The target nuclei is coupled to the sensor via the longitudinal and transversal hyperfine coupling matrix elements  $A_{zz}$  and  $A_{zx}$ . **b** In the qdyne measurement schemes the nuclear precession is consequently probed by the electron spin during the measurement periods  $M_n$ . In our electron-nuclear-double-resonance quantum heterodyne (ENDOR qdyne) protocol the transverse polarization  $I_x$  of the nuclear spin is transferred to the z-axis with a ( $\frac{\pi}{2}$ ) radio frequency (RF) pulse. The nuclear polarization along the z-axis can then be sensed by preparing the sensor electron spin in the superposition state with a ( $\frac{\pi}{2}$ ) pulse and letting it evolve under the effective Hamiltonian  $\hat{S}_z \otimes \hat{I}_z$ , before a second pulse is applied and the sensor is read out. Afterwards the nuclear polarization along the z-axis is transferred back to  $I_x$  via a second RF pulse. Taking the polarization transfer of the nuclear spin due to the RF pulses into account, the effective Hamiltonian of the measurement is given by  $\hat{S}_z \otimes \hat{I}_x$ . In conventional qdyne schemes the (oscillating) transverse polarization of the nuclear spin is sensed directly via microwave (MW) pulse intensive dynamical decoupling (DD) sequences. In our experiment the Knill Dynamical Decoupling (KDD) sequence is used.

components which give rise to fast oscillating signals, we use a phase coherent radio frequency (RF) pulse to convert both components to  $I_z$ . The method proposed and investigated in this work combines previously used electron-nuclear double resonance (ENDOR) methods<sup>12,18</sup> with time efficient signal sampling through quantum heterodyne measurements<sup>9,10,13</sup>. Additionally, we experimentally study the NMR spectral resolution of the protocol and outline its practical application.

## Results and discussion

An isolated nuclear spin in a magnetic field  $B$  precesses freely around the  $z$ -axis with the Larmor frequency  $\omega_L = \gamma_N B$ , where  $\gamma_N$  denotes the nuclear gyromagnetic ratio. As a result, information about  $\omega_L$  can be obtained from the oscillating expectation value of the nuclear spin-1/2 operators  $\hat{I}_x$  and  $\hat{I}_y$ . In a classical qdyne detection scheme the phase information of the time-evolution of e.g.  $\langle \hat{I}_x \rangle$  is sensed by the electronic sensor spin via dynamical decoupling (DD) sequences (see Fig. 1b). These sequences generate an effective Hamiltonian of the form  $\hat{H}_{\text{eff}} \propto \hat{S}_z \otimes \hat{I}_x$ , where  $\hat{S}_z$  is the electron spin operator<sup>19</sup>. This however requires the application of pulses on the timescale of the Larmor frequency  $\omega_L$ , which for protons easily reaches values larger than 100 MHz and hence requires DD pulses with lengths  $< 10$  ns. As of today, this is technically very hard to achieve. In this work, we circumvent the necessity for pulse-intensive DD sequences by mapping the phase information of  $\langle \hat{I}_x \rangle$  to  $\langle \hat{I}_z \rangle$  with a  $3\pi/2$  pulse to the nuclear spin prior to the sensing step. Subsequently, information of  $\langle \hat{I}_z \rangle$  can be sensed by the sensor spin via the effective Hamiltonian of the hyperfine interaction  $\hat{H}_{\text{eff}} = 2\pi A_{zz} \hat{S}_z \hat{I}_z$ . Besides being a static interaction, a further advantage is, that unlike for the direct sensing of  $\langle \hat{I}_x \rangle$ , a rich variety of doubly dressed sensing protocols like ENDOR, DEER<sup>5</sup> or the recently developed DDRF<sup>20</sup> sequences can be applied during the sensing period. After the sensing sequence and successive readout of the electron spin, the nuclear spin is rotated back into the  $x$ - $y$ -plane by application of another  $\pi/2$  pulse, before beginning the next precession period. To enable the correct back-rotation of the nuclear spin into the  $x$ - $y$ -plane, the measurement protocol requires a nuclear phase acquisition of  $\beta = 2\pi k$  ( $k = \text{integer}$ ) during the sensing period. This objective can be accomplished by either resonantly driving the nuclear spin or introducing additional RF  $\pi$  pulses to refocus it during this time. A direct comparison of the DD-based and ENDOR qdyne pulse sequences is shown in Fig. 1. In our experiment a phase coherent RF source with frequency  $\omega_i$  is employed to realize the RF pulses, which effectively translates the nuclear system to the rotating frame of the RF source and converts the precession frequency down, yielding the heterodyne response illustrated in Fig. 2. After a free precession period  $\tau_{\text{fid}}$  and the first  $\pi/2$  pulse of the  $n$ -th measurement cycle  $\langle I_z \rangle$  is given by

$$\langle \hat{I}_z \rangle(n) = \cos((\omega_L - \omega_i)n\tau_{\text{fid}}) \quad (1)$$

By measuring this value weakly<sup>21,22</sup> with the measurement strength  $\alpha$ , the phase information  $(\omega_L - \omega_i)\tau_{\text{fid}}$  is mapped onto the sensor spin with

$$\langle S_z \rangle(n) = -\frac{1}{2} \sin(\alpha) \cos((\omega_L - \omega_i)n\tau_{\text{fid}}), \quad (2)$$

where the back action of the measurement has been neglected. As a result the Larmor frequency of the target spin can be recovered from the readout of  $S_z$  of the sensor spin. A more detailed explanation of the theoretical background of our method and the effects of backaction on our experiment are presented in Supplementary note 2.

**Weak measurement of a single  $^{13}\text{C}$  nuclear spin.** To demonstrate the ENDOR qdyne experiment we probe the spin dynamics of a single weakly coupled  $^{13}\text{C}$  nucleus in the vicinity of the NV center in a proof-of-principle experiment. The coupling strength between the  $^{13}\text{C}$  and the NV sensor reflects the coupling conditions which are also found for sample nuclei on the diamond surface. The interaction of the single  $^{13}\text{C}$  with the NV is given by the hyperfine interaction via a long range dipolar coupling of  $\hat{H} = 2\pi A_{zx} \hat{S}_z \hat{I}_x + 2\pi A_{zz} \hat{S}_z \hat{I}_z$ . Experimentally the  $A_{zx}$  interaction is used to initialize the  $^{13}\text{C}$  nuclear spin via the polarization exchange sequence (pulse-pol)<sup>23</sup>, while the  $A_{zz}$  term is responsible for the signal acquired with our NV center via the proposed scheme. We study a  $^{13}\text{C}$  with hyperfine coupling  $A_{zz} = 6$  kHz. This nucleus was chosen as the coupling is sufficient to get a weak signal within the decoherence time of the sensor ( $T_2^* = 50 \mu\text{s}$ ), while still being smaller than the nuclear Rabi frequency  $\Omega_{^{13}\text{C}} = 15$  kHz. The latter, allows robust RF control of the nuclear spin with respect to the NV center charge and spin state infidelities. The proof of principle experiment follows the sequence shown in Fig. 3a. Due to the limited coherence time of the nuclear carbon spin, the introduction of additional RF  $\pi$  pulses ( $33 \mu\text{s}$ ) into measurement sequence would result in an insufficient number of data points to extract the nuclear spin precession from the experimental data. As a result the experiment is performed with a resonant RF source. The  $^{13}\text{C}$  is initialized via the pulse-pol scheme<sup>23</sup> and is prepared in the superposition state  $|+\gamma\rangle$  with a  $(\pi/2)_{\text{ref}}$ -pulse from the coherent RF source. After a free precession time, the spin is rotated to the measurement basis  $I_z$  via a second pulse  $(3\pi/2)_{\text{ref}+\Phi}$ , where the phase of the following pulses are cycled with a shift of  $\Phi$  along the  $z$ -axis to move the demodulation frequency to 1/4 of the sampling frequency. The  $^{13}\text{C}$   $\langle I_z \rangle$  is mapped with a Ramsey sequence onto the NV sensor spin ( $S_z$ ), which is optically readout. The  $^{13}\text{C}$  is rotated back with  $(\pi/2)_{\text{ref}+\Phi}$ . The protocol is repeated  $M$  times. A detailed description of the experimental design and the data analysis is provided in Supplementary Note 3. In Fig. 3b the experimental result from the described sequence is shown. Fourier transformation of the obtained ENDOR qdyne signal yields a  $^{13}\text{C}$  Larmor frequency of  $2.336 \pm 0.018$  kHz, with a signal decay rate of  $\Gamma = 0.6 \pm 0.1$  kHz. The nuclear  $^{13}\text{C}$  signal is therefore at the expected frequency 2.368 kHz and decays with a rate of  $\Gamma = 0.6 \pm 0.1$  kHz, where the associated spectrum is visualized in Fig. 3c. To further characterize the heterodyne response of our measurement sequence, we also applied it to the  $^{14}\text{N}$  within the NV center (see Supplementary note 2). In the following we analyze the obtained linewidth and compare it to the conventional qdyne measurement (see Fig. 4a, b).

**Linewidth and projected spectral resolution.** Magnetic resonance spectroscopy relies on high spectral resolution which is typically achieved by qdyne experiments on weakly coupled nuclear spins<sup>9</sup>. Our qdyne experiment relies on a modified ENDOR experiment and measures nuclear spins with a rather large hyperfine coupling. Therefore we discuss the impact of coupling strength on the NMR linewidth. We quantify our spectral resolution in comparison to conventional dynamical decoupling based qdyne (conventional qdyne). The interaction between electron and nuclear spin is determined by a static  $A_{zz}$  component and the oscillating component  $A_{zx}$ . At high magnetic fields along the  $z$ -axis  $A_{zz}$  is the dominant term. To quantify the impact of the coupling strength on the observed linewidth, Fig. 4c shows an experimental comparison between ENDOR qdyne and the conventional qdyne. We investigated  $^{13}\text{C}$  nuclei with different  $A_{zz}$  couplings.

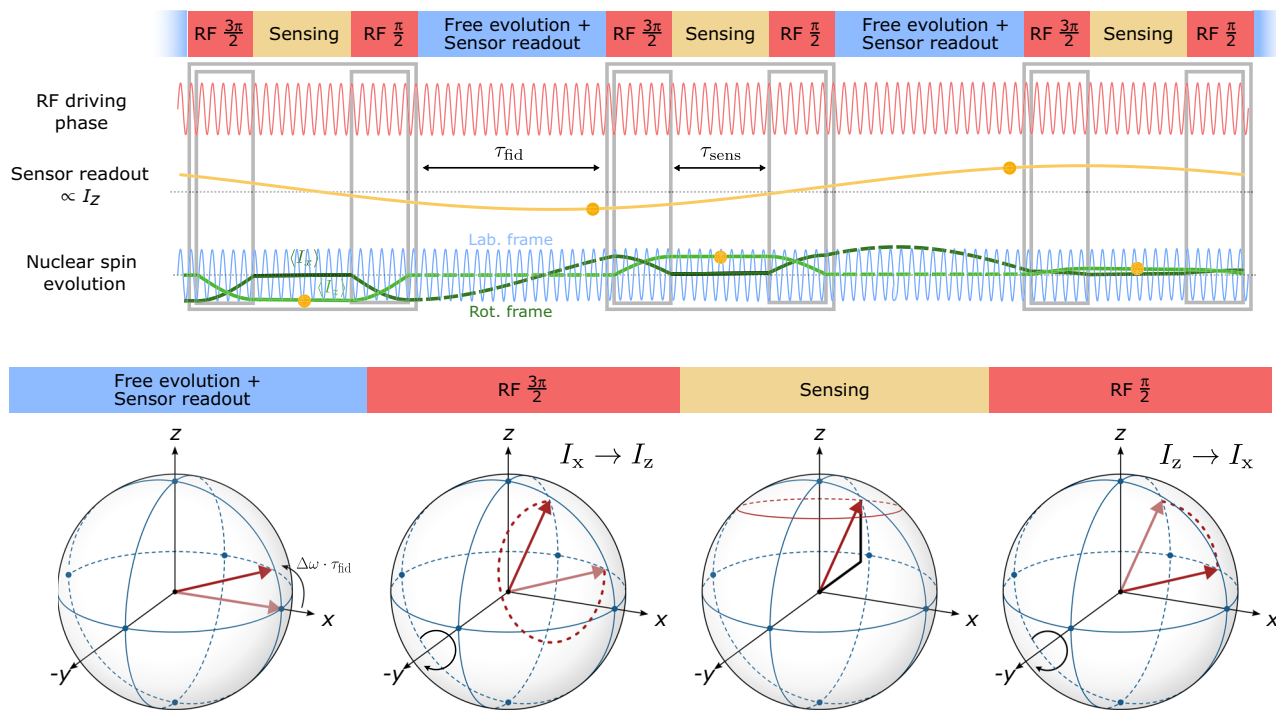


**Fig. 2 Phase evolution of the target spin during the measurement.** The heterodyne detection schemes compares the phase of the Larmor precession of the target spin (blue line) with the phase of the coherent RF driving source (red line). During the free precession time  $\tau_{\text{fid}}$  the nuclear spin acquires a phase of  $\Delta\omega\tau_{\text{fid}}$ , where  $\Delta\omega$  is the detuning of the RF frequency from the Larmor frequency. The phase information (incorporated in  $\langle I_x \rangle$ , dark-green line) is then transferred to the  $I_z$  (green line) and read out via the sensor spin (yellow line) during the time  $\tau_{\text{sens}}$ , before being transferred back to  $I_x$ . The application of a coherent RF pulse enables the effective down-conversion of the nuclear Larmor frequency from  $\omega_L$  to  $\Delta\omega$ . The evolution of the nuclear spin (red arrow) during one representative iteration of the measurement sequence, consisting of free evolution, first RF pulse, sensing period and second RF pulse, is also visualized in the bottom panel.

The decay constant of the conventional qdyne was measured to be  $\Gamma = 1.4 \pm 0.3$  kHz and agrees well with the decay rate of the ENDOR qdyne measurement on the same nuclear spin. As both methods show similar decay rates, we performed an investigation of its origin by studying the decoherence across a large range of  $A_{zz}$  couplings with the conventional qdyne. In Fig. 4c, we compared four  $^{13}\text{C}$  nuclei and find that the three  $^{13}\text{C}$  nuclei with  $A_{zz} > 3$  kHz show a decay rate of about 1 kHz, while only the  $^{13}\text{C}$  nucleus with  $A_{zz} \leq 0.07$  kHz, also discussed in ref. <sup>24,25</sup>, shows a decay rate of  $27 \pm 9$  Hz.

We now discuss the observed decay, i.e. the NMR linewidth. In a diamond crystal with 0.01 %  $^{13}\text{C}$  concentration one expects an intrinsic NMR linewidth of around 10 Hz. In our experiments however, we detect linewidth between 1000 to 27 Hz, depending on the hyperfine coupling. There are multiple effects that cause the observed increase in NMR linewidth. The sequential measurement scheme is based on multiple readout and initialisation sequences during the whole measurement cycle. These sequences involve laser pulses which excite the NV electron spin. In the excited state the electron spin wavefunction is markedly different which causes a change in  $A_{zz}$  hyperfine interaction of the  $^{13}\text{C}$  nucleus<sup>16</sup>. Although the resulting phase error is small because of the short lifetime of the excited state the accumulated total phase error may be substantial because the sequence involved multiple readout steps. Next, charge state switching of the NV between measurements is a possible mechanism. Upon optical excitation the charge and hence spin state of the NV changes between  $\text{NV}^-$  ( $S = 1$ ) and  $\text{NV}^0$  ( $S = 1/2$ ). The known fast nuclear spin relaxation in  $\text{NV}^0$ <sup>8</sup> and the drastic change in spin quantum number leads to a marked increase in nuclear spin relaxation time. Lastly, the initialisation infidelity of the  $\text{NV}^-$  electron spin state<sup>26</sup> can shorten the lifetime<sup>27</sup> of the nuclear spin coherence.

The pulse sequence is designed such that the NV center is initialized in the  $m_s = 0$  state at the beginning of each probing of the nuclear spin state (see Fig. 3a). Any false initialization, which happens with a probability of  $p = 1 - f$  will result in the nuclear spin picking up a large phase error. Here  $f$  denotes the fidelity for the initialization process into the spin state  $m_s = 0$  ( $f \approx 0.9$ ). During the time  $\tau_{\text{meas}}$  between successive measurements shown in Fig. 1b the effective change in the nuclear Larmor frequency is 6.0 kHz which results in a phase difference of  $A_{zz}\tau_{\text{meas}} = 0.63$  rad with the probability  $1 - f$ . When averaging the recorded nuclear spin precession over multiple measurement cycles, the random phase shifts introduce a decay of the coherent nuclear precession, yielding an exponentially decaying cosine signal with an effective decay rate  $\Gamma$ , given by

$$\Gamma = \frac{2(1-f)\sin^2(A_{zz}\tau_{\text{meas}})}{\tau_{\text{meas}}} \quad (3)$$

as derived in Supplementary note 5. A quantitative study of the relation between decay rate  $\Gamma$  and the measurement time  $\tau_{\text{meas}}$  is given in Supplementary note 6. Some insight on the importance of the three mechanisms come from an analysis of Fig. 4c. The figure shows the measured nuclear spin relaxation rate as a function of the nuclear hyperfine coupling. The first two mechanisms scale with  $(A_{zz})^2$ , as they originate from a random walk, and therefore cannot explain the observed functional behaviour. Only the decoherence mechanism based on spin initialisation infidelity is in the right order of magnitude ( $\approx 1$  kHz for  $A_{zz} = 6$  kHz,  $\tau_{\text{meas}} = 105 \mu\text{s}$  and  $f = 0.9$ ) and shows a functionality which is similar to the observed dependence, see Supplementary note 5.

Independent of the exact description of the mechanisms for decoherence, the comparison between conventional qdyne and

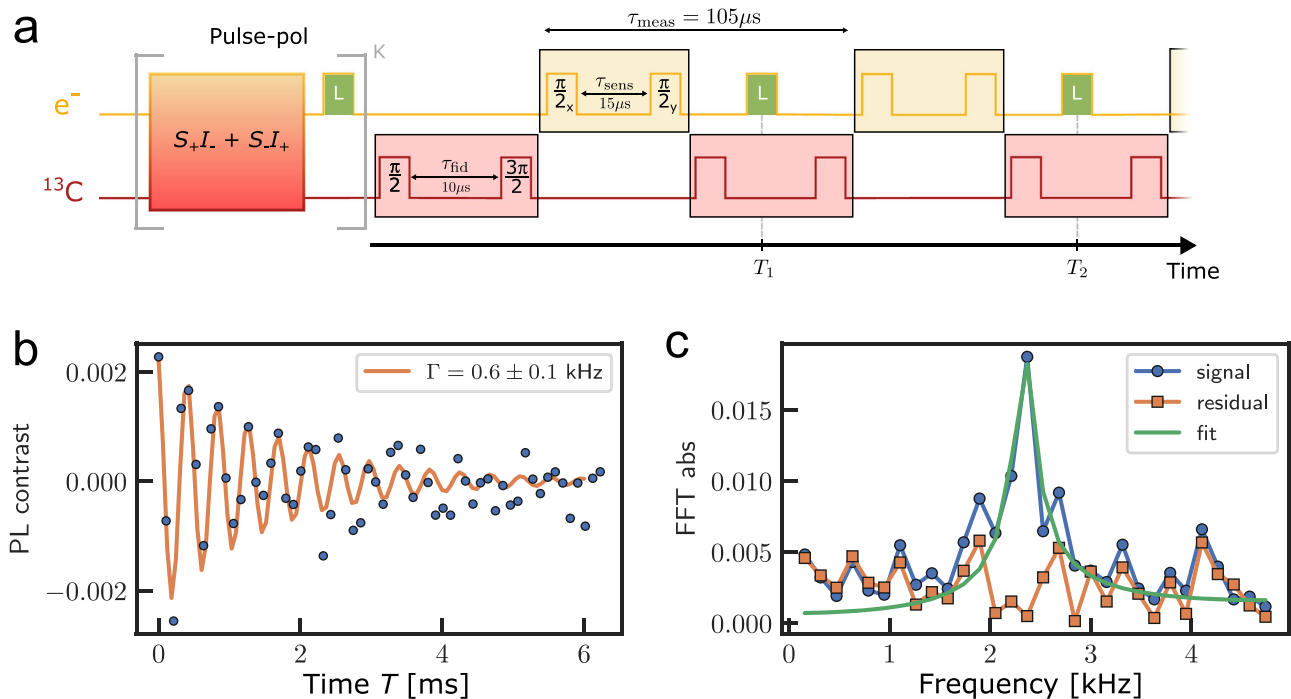


**Fig. 3 Proof of principle experiment with a single  $^{13}\text{C}$  spin and a single NV center.** **a** Sensing sequence of the proof of principle experiment. The  $^{13}\text{C}$  spin is hyperpolarized with the pulse-pol sequence before the nuclear spin precession is initiated with a  $(\pi/2)_{\text{ref}}$  pulse from the reference RF source. The nuclear spin evolves freely during  $\tau_{\text{fid}}$  ( $10\ \mu\text{s}$ ) and gets rotated to the z-basis with a second  $(\pi/2)_{\text{ref}}$  pulse from the same source. The z-component of the polarization is measured with a Ramsey sequence on the sensor spin  $((\pi/2)_x - (\pi/2)_y)$  during  $\tau_{\text{sens}}$  ( $15\ \mu\text{s}$ ) and the sensor spin is readout with a laser pulse at time  $T_i$ . Finally the nuclear spin is rotated back with a  $(3\pi/2)_{\text{ref}}$  pulse, continuing its free evolution. The Rabi period of the applied RF pulses is  $66\ \mu\text{s}$ . Inclusion of the repolarization time ( $2.5\ \mu\text{s}$ ), readout time ( $1.9\ \mu\text{s}$ ) and an additional wait time ( $10\ \mu\text{s}$ ) after the RF pulse leads to a sampling time of  $105.5\ \mu\text{s}$ . **b** Experimental measurement of the nuclear evolution under the protocol above at resonance. The experimental time trace (blue) is fitted by an exponentially decaying cosine (orange). For the proof of principle the free evolution of the target spin was implemented as a phase shift in the  $3\pi/2$  pulse with  $\Phi = \pi/2$ , leading to a normalized signal periodicity of  $4 \times 105.5\ \mu\text{s}$ . The decay rate of the signal is  $\Gamma = 0.6 \pm 0.1\ \text{kHz}$ . The spectrum of the signal with a peak at  $2.368\ \text{kHz}$  is shown in **c** (blue) alongside the Fourier spectrum of the fit (green) and the residuals of the fit (orange) from **b**.

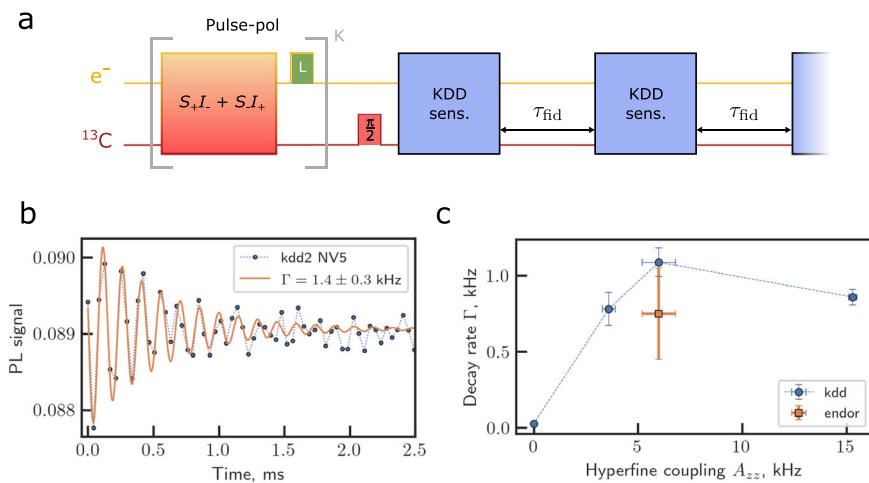


**Fig. 4 Decay rate comparison to conventional dynamical-decoupling-based heterodyne detection.** **a** Conventional dynamical decoupling (DD)-based heterodyne detection protocol<sup>22,34</sup>. The  $^{13}\text{C}$  spin is hyperpolarized with the pulse-pol sequence and the nuclear spin precession is initiated with a  $(\pi/2)_{\text{ref}}$  pulse from the reference radio frequency (RF) source. The nuclear spin evolves freely while interacting with the sensor spin through a Knill-Dynamical-Decoupling (KDD) sequence during the sensing block (blue) and the free evolution time  $\tau_{\text{fid}}$  (see Fig. 1b). The sensor is readout with a laser pulse and a wait time is added to adjust the total sequence time (see Supplementary Note 4). This block is repeated  $M$  times. **b** Conventional quantum heterodyne (qdyne) signal (blue) from the sequence above with a decay rate of  $\Gamma = 1.4 \pm 0.3\ \text{kHz}$  from the exponentially decaying cosine fit (orange). **c** Comparison of the measurement back-action corrected lifetimes for different NV- $^{13}\text{C}$  pairs with conventional qdyne (blue) and electron-nuclear-double-resonance (ENDOR) qdyne (orange). The lowest decay rate of  $27 \pm 9\ \text{Hz}$  appears in the NV- $^{13}\text{C}$  pair with  $A_{zz} \leq 70\ \text{Hz}$ .

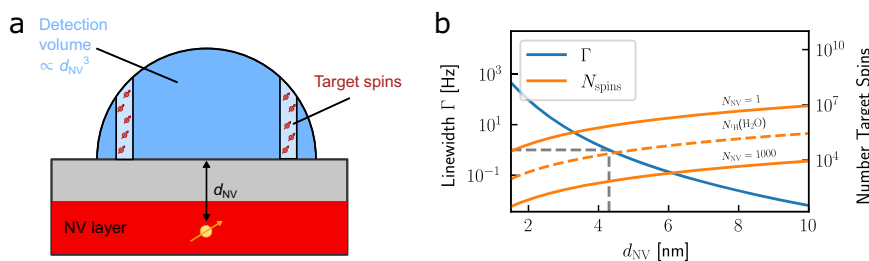


**Fig. 5 Outlook for the application of the ENDOR qdyne detection scheme.** **a** Schematic of the extension of the sensing scheme to sample detection. Only the target spins with sufficient  $A_{zz}$  coupling (red spins) will be detected by our measurement scheme. **b** Relation between implantation depth of the NV centers and the detected linewidth. By increasing the depth of the NV centers, the dipolar coupling via  $A_{zz}$  decreases, resulting in a decreasing linewidth of the ENDOR qdyne protocol (see Eq. (3)). For example, a linewidth of 1 Hz is predicted at  $d_{NV} = 4.2$  nm for  $^1\text{H}$  target spins (grey line). However, as the  $A_{zz}$  coupling decreases, the number of detected target spins has to increase to maintain sufficient signal quality. The orange lines represent the necessary number of detected  $^1\text{H}$  target spins to reach a SNR of 3 in a 10 min measurement cycle with 100 points. For the case of  $d_{NV} = 4.2$  nm  $10^4$  target spins in the detection volume are sufficient if a NV ensemble of 1000 sensor spins is used. This can easily be achieved, as the dashed orange line shows the number of  $^1\text{H}$  target spins of a water sample in the detection volume of the sensor when thermal polarization in a 3 T bias field is considered.

ENDOR qdyne yields that the spectral resolution limits are similar. We find that qdyne, can measure very small  $A_{zz} \rightarrow 0$ , resulting in a sensor unlimited spectral resolution below 30 Hz. Such small couplings are hard to reach by ENDOR qdyne because for measurements on single nuclear spins the phase provided by  $A_{zz}\tau_{sens}$  needs to be large enough to result in a sufficient change in the electron spin sensor readout signal. As we are using an electron spin Ramsey sequence the time for acquiring this phase is limited by the electron  $T_2^*$ , i.e. around 10  $\mu\text{s}$ . The resulting phase difference is too small to be detected for small  $A_{zz}$  couplings. This is intrinsically different from the DD detection of NMR where the interaction time is around 1ms. However, in the case of a small ensemble of nuclear spins, the ENDOR qdyne could be advantageous (see Fig. 5). Distant ensembles of weakly coupled nuclear spins are desirable for high spectral resolutions in nanoscopic surface NMR experiments. In these cases the  $A_{zz}$  coupling strength typically coincides with the performance range of ENDOR qdyne. For example, an  $A_{zz}$  coupling below 70 Hz is reached when the  $^{13}\text{C}$  ( $^1\text{H}$ ) is  $\approx 4.5$  nm ( $\approx 7$  nm) away from the NV center along the z axis. The loss of coupling strength and therefore signal size has to be compensated by sensing an ensemble of nuclear spins with an ensemble of NV centers, as already applied with conventional qdyne in ref. 13,28.

A detailed investigation into the trade-off between achieved sensitivity and magnetic susceptibility for our system is given in Supplementary note 6.

## Conclusions

In summary we presented a nanoscale NMR protocol that is based on a heterodyne measurement via double resonance. Hereby the advantages of heterodyne sensing schemes are adjusted to enable application in high-field scenarios. We showed weak measurements of a single  $^{13}\text{C}$  nuclear spin with our protocol. The extracted linewidth was compared to conventional qdyne methods and we found that the linewidth is intrinsically limited. Finally we discussed the effective sensitivity of heterodyne sensing and the service costs involved. The experimental demonstration of the proposed protocol under high magnetic fields to verify the predicted advantage over DD-based methods requires further work.

Double resonance qdyne is particular interesting for nano- to micron-scale NMR sensing scenarios, outlined in Figs. 1a and 5. In this scenario, an ensemble of nuclear spins is coupled to the NV sensor spins<sup>13,28</sup>. This means that the linewidth is not affected by the hyperfine dynamics like in our demonstrator experiment and the same spectral resolution as conventional qdyne can be achieved. In the future, ENDOR qdyne could be

combined with echo-type measurement schemes<sup>18</sup> or homo- and heteronuclear decoupling sequences<sup>29</sup> improving the spectral resolution for solids and dipolar interacting samples. The removed constraints on the microwave power allow us to apply this method to high magnetic fields, e.g. optical detected magnetic resonance with NVs at 8 T<sup>30</sup>. A high magnetic field leads to an increased thermal polarization equal to larger signals or equivalently reduced sensing volumes<sup>14</sup>. Additionally, the sensitivity to chemical shifts increases, allowing to study of proteins or short-lived molecules<sup>31</sup>. In the preparation of the manuscript, we became aware of a similar theoretical work<sup>32</sup>. In the future, the measurement block of our protocol could be extended to the more advanced double resonance schemes e.g. proposed in the recent work<sup>32</sup> and combined with multidimensional sequences (e.g. COSY<sup>33</sup>).

## Methods

**Experimental setup.** The experiments were conducted with a confocal room temperature single NV setup depicted in Supplementary Fig. 1. The NV is excited in the phonon sideband with a green 520 nm laser. This initializes and readouts the NV electron spin state. The red fluorescence of the NV is detected with an avalanche photo diode (APD) before passing through a wedged mirror, a pinhole 50  $\mu\text{m}$  and a long pass filter 650 nm. The diamond sample is a 2 mm  $\times$  2 mm  $\times$  80  $\mu\text{m}$ , (111)-oriented polished slice from a  $^{12}\text{C}$ -enriched (99.995 %) diamond crystal. The crystal was grown by the temperature gradient method under high-pressure high-temperature conditions at 5.5 GPa and 1350  $^\circ\text{C}$ , using high-purity Fe-Co-Ti solvent and high-purity  $^{12}\text{C}$ -enriched solid carbon. The single NV centers were created from intrinsic nitrogen by irradiation with 2 MeV electrons at room temperature with a total fluence of  $1.3 \cdot 10^{11} \text{ cm}^{-2}$  and annealed at 1000  $^\circ\text{C}$  (for 2 h in vacuum). The typical lifetimes for the NV centers in this slice are  $T_2^* = 50 \mu\text{s}$  and  $T_2 \approx 300 \mu\text{s}$ <sup>15,21</sup>. The diluted  $^{13}\text{C}$  bath in the lattice leads to a electron  $T_2^*$  time of 50  $\mu\text{s}$  and usually only one  $^{13}\text{C}$  is significantly coupled to a single NV center. The nuclear and electron spins are manipulated with an arbitrary waveform generator, able to sample 12 GSamples/s, with two channels. The MW channel is amplified with a Hughes-Traveling Wave Tube 8010H amplifier (TWT, max. 7 MHz Rabi frequency), while the RF channel is amplified with Amplifier Research 150A250. They are combined with a combiner before the both connect to the coplanar waveguide where the diamond is glued to. We use a 3 axis piezo-positioner stage (range 100  $\times$  100  $\times$  25 ( $\mu\text{m}$ )<sup>3</sup>) from npoint. This allows us to keep a single NV in focus. The setup of the experiment is visualized in Supplementary Note 1.

For the proof of principle we searched for a single NV center with a moderate  $^{13}\text{C}$  with  $A_{zz}$  coupling with a stimulated echo sequence<sup>8</sup>. Moderate means that the coupling is smaller than the RF Rabi frequency for  $^{13}\text{C}$  of 15 kHz, while still being strong enough coupled to address it within the  $T_2^*$  time. We found NV#5 which has a coupling of  $A_{zz} = 6$  kHz. For the comparison of the natural linewidth we studied other NV centers within the  $100 \times 50 \times 5$  ( $\mu\text{m}$ )<sup>3</sup> volume. A list of all used variables can be found in Supplementary Note 7.

### Data availability

Data supporting the findings of this study are available in a public data repository under following link: <https://doi.org/10.18419/darus-3728>.

Received: 17 April 2023; Accepted: 5 October 2023;

Published online: 17 October 2023

### References

- Ernst, R. R. Nuclear magnetic resonance fourier transform spectroscopy. *Biosci. Rep.* **12**, (1992).
- Casey, W. H., Wang, Z., Brandt, N. & Curro, N. The promise of optical nmr spectroscopy for experimental aqueous geochemistry. *Am. J. Sci.* **320**, 533–545 (2020).
- Souza, A. M., Álvarez, G. A. & Suter, D. Robust dynamical decoupling. *Philos. Trans. R. Soc. A: Math., Phys. Eng. Sci.* **370**, 4748–4769 (2012).
- Casanova, J., Wang, Z.-Y., Schwartz, I. & Plenio, M. B. Shaped pulses for energy-efficient high-field nmr at the nanoscale. *Phys. Rev. Appl.* **10**, 044072 (2018).
- Schweiger, A. & Jeschke, G. *Principles of pulse electron paramagnetic resonance* (Oxford University Press on Demand, 2001).
- Laraoui, A. et al. High-resolution correlation spectroscopy of  $^{13}\text{C}$  spins near a nitrogen-vacancy centre in diamond. *Nat. Commun.* **4**, 1651 (2013).
- Staudacher, T. et al. Nuclear magnetic resonance spectroscopy on a (5-nanometer)  $^3$  sample volume. *Science* **339**, 561–563 (2013).
- Pfender, M. et al. Nonvolatile nuclear spin memory enables sensor-unlimited nanoscale spectroscopy of small spin clusters. *Nat. Commun.* **8**, 1–12 (2017).
- Schmitt, S. et al. Submillihertz magnetic spectroscopy performed with a nanoscale quantum sensor. *Science* **356**, 832–837 (2017).
- Boss, J. M., Cujia, K., Zopes, J. & Degen, C. L. Quantum sensing with arbitrary frequency resolution. *Science* **356**, 837–840 (2017).
- Zaiser, S. et al. Enhancing quantum sensing sensitivity by a quantum memory. *Nat. Commun.* **7**, 1–11 (2016).
- Aslam, N. et al. Nanoscale nuclear magnetic resonance with chemical resolution. *Science* **357**, 67–71 (2017).
- Glenn, D. R. et al. High-resolution magnetic resonance spectroscopy using a solid-state spin sensor. *Nature* **555**, 351–354 (2018).
- Schwartz, I. et al. Blueprint for nanoscale nmr. *Sci. Rep.* **9**, 1–11 (2019).
- Meinel, J. et al. Heterodyne sensing of microwaves with a quantum sensor. *Nat. Commun.* **12**, 1–8 (2021).
- Chu, Y. et al. Precise spectroscopy of high-frequency oscillating fields with a single-qubit sensor. *Phys. Rev. Appl.* **15**, 014031 (2021).
- Staudenmaier, N., Schmitt, S., McGuinness, L. P. & Jelezko, F. Phase-sensitive quantum spectroscopy with high-frequency resolution. *Phys. Rev. A* **104**, (2021).
- Mamin, H. et al. Nanoscale nuclear magnetic resonance with a nitrogen-vacancy spin sensor. *Science* **339**, 557–560 (2013).
- Ma, W.-L. & Liu, R.-B. Angstrom-resolution magnetic resonance imaging of single molecules via wave-function fingerprints of nuclear spins. *Phys. Rev. Appl.* **6**, 024019 (2016).
- Bradley, C. E. et al. A ten-qubit solid-state spin register with quantum memory up to one minute. *Phys. Rev. X* **9**, 031045 (2019).
- Pfender, M. et al. High-resolution spectroscopy of single nuclear spins via sequential weak measurements. *Nat. Commun.* **10**, 1–8 (2019).
- Cujia, K., Boss, J. M., Herb, K., Zopes, J. & Degen, C. L. Tracking the precession of single nuclear spins by weak measurements. *Nature* **571**, 230–233 (2019).
- Schwartz, I. et al. Robust optical polarization of nuclear spin baths using hamiltonian engineering of nitrogen-vacancy center quantum dynamics. *Sci. Adv.* **4**, eaat8978 (2018).
- Meinel, J. et al. Quantum nonlinear spectroscopy of single nuclear spins. *Nat. Commun.* **13**, 5318 (2022).
- Vorobyov, V. V. et al. Transition from quantum to classical dynamics in weak measurements and reconstruction of quantum correlation. *Phys. Rev. A* **107**, 042212 (2023).
- Song, Y. et al. Pulse-width-induced polarization enhancement of optically pumped nv electron spin in diamond. *Photonics Res.* **8**, 1289–1295 (2020).
- Maurer, P. C. et al. Room-temperature quantum bit memory exceeding one second. *Science* **336**, 1283–1286 (2012).
- Liu, K. S. et al. Surface nmr using quantum sensors in diamond. *Proc. Natl Acad. Sci.* **119**, (2022).
- Waugh, J. S., Huber, L. M. & Haeberlen, U. Approach to high-resolution nmr in solids. *Phys. Rev. Lett.* **20**, 180 (1968).
- Fortman, B. et al. Electron–electron double resonance detected nmr spectroscopy using ensemble nv centers at 230 ghz and 8.3 t. *J. Appl. Phys.* **130**, 083901 (2021).
- Lovchinsky, I. et al. Nuclear magnetic resonance detection and spectroscopy of single proteins using quantum logic. *Science* **351**, 836–841 (2016).
- Munuera-Javaloy, C., Tobalina, A. & Casanova, J. High-resolution nmr spectroscopy at large fields with nitrogen vacancy centers. *Phys. Rev. Lett.* **130**, 133603 (2023).
- Smits, J. et al. Two-dimensional nuclear magnetic resonance spectroscopy with a microfluidic diamond quantum sensor. *Sci. Adv.* **5**, eaaw7895 (2019).
- Cujia, K. S., Herb, K., Zopes, J., Abendroth, J. M. & Degen, C. L. Parallel detection and spatial mapping of large nuclear spin clusters. *Nat. Commun.* **13**, 1260 (2022).

### Acknowledgements

We acknowledge financial support by European Union's Horizon 2020 research and innovation program ASTERIQS under grant No. 820394, European Research Council advanced grant No. 742610, SMel, Federal Ministry of Education and Research (BMBF) project MiLiQuant and Quamapolis, the DFG (FOR 2724), the Max Planck Society, and the Volkswagentiftung.

### Author contributions

J.M. and V.V. came up with the initial idea of the experiment, and designed the experiment. J.M., V.V., M.K. and J.W. performed the initial experiment, J.M., V.V. and J.W. analyzed the experimental data, J.M., R.M. and V.V. performed additional required experiments and numerical simulations. D.D. provided theoretical support. H.S., S.O. and J.I. manufactured and characterised the diamond sample. V.V., J.M., R.M. and J.W. wrote the text of the manuscript. All authors read and commented on the manuscript.

### Funding

Open Access funding enabled and organized by Projekt DEAL.

### Competing interests

The authors declare no competing interests.

### Additional information

**Supplementary information** The online version contains supplementary material available at <https://doi.org/10.1038/s42005-023-01419-2>.

**Correspondence** and requests for materials should be addressed to Vadim Vorobyov.

**Peer review information** *Communications Physics* thanks Jeong Hyun Shim and the other, anonymous, reviewer(s) for their contribution to the peer review of this work.

**Reprints and permission information** is available at <http://www.nature.com/reprints>

**Publisher's note** Springer Nature remains neutral with regard to jurisdictional claims in published maps and institutional affiliations.



**Open Access** This article is licensed under a Creative Commons Attribution 4.0 International License, which permits use, sharing, adaptation, distribution and reproduction in any medium or format, as long as you give appropriate credit to the original author(s) and the source, provide a link to the Creative Commons licence, and indicate if changes were made. The images or other third party material in this article are included in the article's Creative Commons licence, unless indicated otherwise in a credit line to the material. If material is not included in the article's Creative Commons licence and your intended use is not permitted by statutory regulation or exceeds the permitted use, you will need to obtain permission directly from the copyright holder. To view a copy of this licence, visit <http://creativecommons.org/licenses/by/4.0/>.

© The Author(s) 2023